WARSAW UNIVERSITY OF TECHNOLOGY Index 351733
FACULTY OF CIVIL ENGINEERING
COMMITTEE FOR CIVIL AND WATER ENGINEERING
POLISH ACADEMY OF SCIENCES ISSN 1230-2945

DOI: 10.24425/ace.2026.157458

ARCHIVES OF CIVIL ENGINEERING

Vol. LXXII ISSUE 1 2026

pp. 23–40

Research paper

Study on fracture patterns in moderately weathered granite due to blasting damage using the shock wave Coupled Eulerian–Lagrangian simulation method

Mingyue Ma[1], Yajun Liu[2], Zhihong Duan[3], Yang Zheng[4], Fengting Li[5]

Abstract: Depth gradients, which arise from variations in geostress at different strata, lead to rapid alterations in the internal stress state of rocks during blasting operations. These changes contribute to heterogeneities in rock strength and blast resistance, thereby presenting potential risks to engineering safety. To understand the damage and fracture patterns typically observed in granite blasting activities within underground engineering projects, we created a series of rectangular six-hole models using the advanced finite element software ABAQUS. By utilizing the Coupled Eulerian–Lagrangian (CEL) technique, the model distinguished between Eulerian parts, segmented into domains, and Lagrangian elements; the Eulerian domain was designated as air, while the Lagrangian section was characterized by TNT to mimic the shock wave propagation following detonation. This research scrutinizes the geostress conditions of granite across varying depth gradients, elucidates the extent and severity of granite impairment induced by blasting, and furnishes innovative viewpoints and methodologies for examining rock damage mechanisms in blasting engineering.

Keywords: blasting, granite, damage and fracturing, CEL simulation

[1]PhD., Shandong Boshuo Geotechnical Engineering Design Consulting Co., Ltd., AI. No. 588 Jing Qi Road, Jinan, China, e-mail: hssdu@163.com, ORCID: 0009-0000-6903-0935

[2]PhD., Shandong University, School of Civil Engineering, Al. No. 17922, Jingshi Road, Jinan, China, e-mail: 1719562625@qq.com, ORCID: 0009-0004-0965-6708

[3]PhD., PowerChina Municipal Construction Group Co., Ltd., Al. No. 2 Haitai Development Five, Tianjin, China, e-mail: 2339520268@qq.com, ORCID: 0009-0005-3578-1323

[4]PhD., Shandong University, School of Civil Engineering, Al. No. 17922, Jingshi Road, Jinan, China, e-mail: 1010073862@qq.com, ORCID: 0000-0002-6014-4124

[5]PhD., Shandong University, School of Civil Engineering, Al. No. 17922, Jingshi Road, Jinan, China, e-mail: 1025394655@qq.com, ORCID: 0000-0002-8995-7479

1. Introduction

As urbanization accelerates in China and economic development continues to thrive, the construction of subway systems is rapidly advancing. Subways serve as an integral component of urban public transportation, offering significant relief to vehicular congestion and fostering comprehensive socio-economic growth [1]. The excavation process for subway stations presents a technically demanding engineering challenge, particularly when conducted in hard rock environments like granite. Blasting operations in these conditions are fraught with complexities due to the high density and strength of granite, which impede efficient blasting. Furthermore, the inherent cracks and joints within granite can produce unforeseeable fracture propagation during blasting [2], compromising the stability of the surrounding rock mass at subway stations. In engineering practices, these intricacies often result in instances of overblasting or underblasting, where the blasting outcome deviates from the planned objectives, leading to potential safety risks and financial losses.

The advancement of computational mechanics and numerical simulation technologies has paved the way for a deeper comprehension of blasting cracking mechanisms through numerical studies employing high-performance software like LS-DYNA and ABAQUS. One novel fracture model was introduced to replicate blasting fractures in granite, and by experimentally calibrating the model parameters, they furnished new tools for numerical simulations of rock materials [3]. The precision of the RHT model parameters were ascertained via repeated blasting experiments and probed the influence of geostress on rock failure behavior using numerical simulations. The findings revealed that confinement significantly alters the failure mode of granite samples, with cracks predominantly extending along the maximum principal stress direction [4]. The granite blasting cracks using LS-DYNA software was emulated, integrating the RHT and HJC models, and proposed refined failure criteria, suggesting that the RHT model is more suitable for addressing cyclic blasting issues [5]. The JH-2 model was adopted as the constitutive model for rock materials in tunnel smooth blasting and introduced a straightforward method to determine model parameters, effectively estimating rock blasting damage, though the validation of material damage parameters was not included [6]. The JH-2 model parameters for dolomite were determined by synthesizing experimental and literature data, highlighting that certain material parameters correlate with element size and necessitate adjustment according to the dimensions and configuration of the actual problem. These investigations offer valuable insights for refining blasting designs and forecasting blasting outcomes [7]. A two-dimensional double-hole blasting simulation study was conducted by using ANSYS/LS-DYNA, focusing on explosive efficiency and blasting effects in mining operations. Starting with the compatibility of explosives with rock, the study identified the most appropriate type of Cyclotol explosives and blasting parameters for granite, achieving optimal blasting results [8]. The blasting effect was studied by using four experimental modes with different cutting forms due to the cutting forms. And the influences of the borehole space and the blasting delay were discussed [9]. In summary, the simulation of blasting-induced rock damage serves as a crucial engineering technique. It is instrumental not only in deciphering complex phenomena during blasting but also in enhancing the safety and economic efficiency of construction projects. As technology continues to evolve, this technique is poised to play an even more pivotal role in future engineering endeavors.

To address this objective, the present study draws upon the tunneling blasting project of Danshan Subway Station on Qingdao Metro Line 15. It concentrates on the patterns of cracking and damage that occur during the blasting construction process of moderately weathered and slightly weathered granite. Utilizing the comprehensive finite element package ABAQUS, a series of rectangular six-hole models were developed. By employing the Coupled Eulerian–Lagrangian (CEL) technique, simulations of shock wave propagation through space following explosive detonation were performed. This research investigates the geostress conditions of granite across varying depth gradients, assesses the extent and severity of granite impairment induced by blasting, and offers fresh perspectives and techniques for probing the mechanisms of rock damage caused by blasting in engineering projects.

2. Project overview

Danshan Station on Qingdao Metro Line 15 is an underground two-level island-style tunnel station encompassing a total length of 215 meters and a standard cross-sectional width of 21.1 meters. The station spans a total construction area of 16,877 square meters. Auxiliary structures at the station include three entrances and exits, two ventilation pavilions, one accessible elevator, and one emergency exit. The subway station features a large cross-sectional tunnel structure that is constructed using smooth blasting techniques, while the primary structure employs the "top-down" initial support arch cover method. The tunnel body of the station predominantly resides within moderately weathered and slightly weathered granite zones, with overburden thicknesses ranging from 15.9 to 19.6 meters. Vertically, the rock mass can be categorized into highly weathered, moderately weathered, and slightly weathered strata. The engineering tunnel mainly exists within the Laoshan period's moderately weathered and slightly weathered granite zones, boasting overburden thicknesses of 15.9 to 19.6 meters, a vast excavation span (21.4 to 22.6 meters), and clear heights (17.75 to 18.1 meters). The volume of rock blasted during the project reached 120,052.31 cubic meters; the bedrock surface is relatively elevated, with overburden thicknesses of 13.7 to 15.8 meters (arch crown burial depths of 15.5 to 19.5 meters), and the slightly weathered granite overburden thickness at the arch crown is approximately 2 to 10 meters. The surrounding rock is comparatively fragmented, classified between grades III to V, with the main structure entirely situated within the slightly weathered granite layer. The basic mechanical parameters of granite are shown in Table 1.

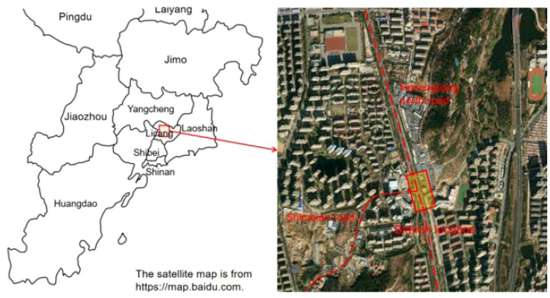

Fig. 1. Plan of Danshan Station, Qingdao Metro

Table 1. Basic parameters of granite

Granite	P **(kg/m^3)**	***E*** **(GPa)**	***υ***	***G*** **(GPa)**	***T*** **MPa**	***K***	***C*** **MPa**	V_p **(km/s)**	***Vs*** **(km/s)**	***Rc*** **(MPa)**
Slight weathering	2540	31.01	0.18	12.31	3.5	44.65	1.41	3.54	1.98	113.51
Moderate weathering	2520	15.63	0.26	6.62	2.3	30.01	1.41	3.06	1.63	53.87

3. Numerical calculation models and analysis methods

To explore the typical damage and cracking patterns observed during granite blasting operations in underground engineering projects, the following methodology is adopted: Firstly, utilizing the scatter plot of geostress distribution with depth for igneous, sedimentary, and metamorphic rocks as proposed by Jingfeng, and in conjunction with the depth of the granite layers at Qingdao Danshan Subway Station, the geostress values for granite at varying depths are calculated. Secondly, the comprehensive finite element software package ABAQUS is employed to develop a series of rectangular six-hole models. By applying the Coupled Eulerian–Lagrangian (CEL) technique, the simulation of shock wave propagation through space following explosive detonation is performed. Thirdly, an analysis is conducted on the geostress conditions of granite across different depth gradients to examine the extent and severity of granite degradation and fragmentation induced by blasting.

3.1. Geostress

JING Feng collected a substantial amount of measured geostress data from mainland China and established scatter plots of geostress distribution with depth for igneous, sedimentary, and metamorphic rocks. He conducted regression analyses according to their respective distribution patterns [10]. The stress calculation formula applicable to granite is as follows:

$$\sigma_1 = 0.0318H + 5.895 \tag{3.1}$$

$$\sigma_2 = 0.0198H + 0.232 \tag{3.2}$$

where H is depth.

In this study, the rock layer depth at Qingdao Danshan Station primarily ranges from 15 to 20 meters, with the arch crown buried at depths of 15.5 to 19.5 meters; the overburden thickness is 13.7 to 15.8 meters. A depth of 20 meters is used to represent the typical depth for subway blasting construction, while a range of 200 to 1000 meters represents the typical excavation depth for mountain tunnels in China. The calculations for confining pressures at different depths are shown in Table 2. The calculations indicate that $\sigma_1 = 6.53$ MPa, $\sigma_2 = \sigma_3 = 0.63$ MPa.

Table 2. Three dimensional stress at different depths

Depth (m)	σ_1 (MPa)	σ_2 (MPa)	σ_3 (MPa)
20	6.53	0.63	0.63
200	12.25	4.19	4.19
500	21.79	10.13	10.13
1000	37.69	20.03	20.03

3.2. Numerical calculation model

3.2.1. Rock mass model

In the numerical simulation, it is assumed that the granite rock mass is homogeneous and isotropic. The rock blasting model is shown in Figure 2. The dimensions of the rock mass model are $6.0 \times 2.0 \times 3.0$ m. To more realistically simulate the double-side guide wall pit blasting method, six blastholes are set in the rock mass, with a lateral spacing of 2.0 m and a longitudinal spacing of 1.0 m; the blastholes are designed as cylindrical spaces with a radius of 0.6 m and a depth of 2 m. The model element type is the Lagrangian element (C3D3R), with a grid density of 0.02 m in the X–Y plane. Considering the computational capacity of the computer, the grid on the Z-axis is appropriately simplified with a density set at 0.08 m, totaling 2,073,568 elements.

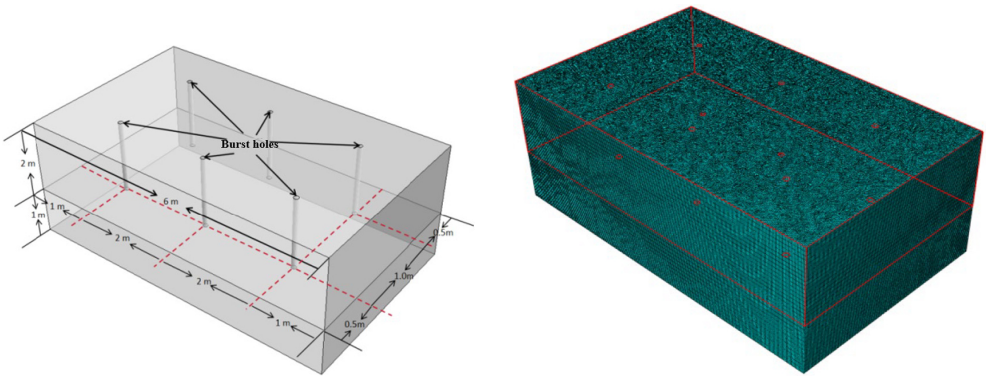

(a) (b)

Fig. 2. Rock mass model for six hole blasting: (a) Size Setting, (b) Meshing

The thesis utilizes the JH-2 model to simulate granite. The JH-2 model, developed by Holmquist and Johnson in 2001, is designed to describe the brittle response of materials like ceramics [11–15]. Specifically created for simulating the behavior of brittle materials such as ceramics and rocks under high strain rates and high pressures, the JH-2 model is an advanced constitutive model with significant advantages in handling material responses under extreme

conditions like explosions or high-speed impacts. This model accurately describes the complex behaviors of brittle materials under high strain rates and pressures, including the rapid initiation and propagation of cracks. Furthermore, the JH-2 model is particularly suited for simulating the failure and fragmentation behaviors of brittle materials, which is crucial for understanding and predicting material responses during blasting processes. The theory related to the JH-2 model has been discussed in detail in the literature [16].

3.2.2. Eulerian Body

In this study, the Coupled Eulerian–Lagrangian (CEL) method is used to divide the Eulerian components into Eulerian domains and Lagrangian elements. In ABAQUS, the Coupled Eulerian–Lagrangian (CEL) method [17] can better handle scenarios involving complex materials interacting under high strain rates and high pressures. To implement CEL simulations in ABAQUS, it is first necessary to precisely define the properties of explosives, air, and other solid structures [18]. The geometric model distinguishes between Eulerian domains (fluids or flowable materials) and Lagrangian domains (solid structures). By setting the Eulerian domain as air material and the Lagrangian domain as TNT, the propagation of shock waves in space after an explosive blasting can be simulated.

The model is shown in Figure 3, where the Eulerian domain measures $10 \times 6 \times 4$ m. The TNT is positioned in the middle of the Eulerian domain as a cylindrical body measuring 0.05×2 m, placed at the center of the blasthole in the rock mass model. The simulation starts with millisecond delay blasting from the center to the sides, with an interval time of 1 ms. TNT and air are modeled using eight-node reduced integration Eulerian elements (EC3D8R). Non-reflecting boundary conditions are set for the Eulerian domain edges to eliminate reflections caused by shock waves contacting the boundaries.

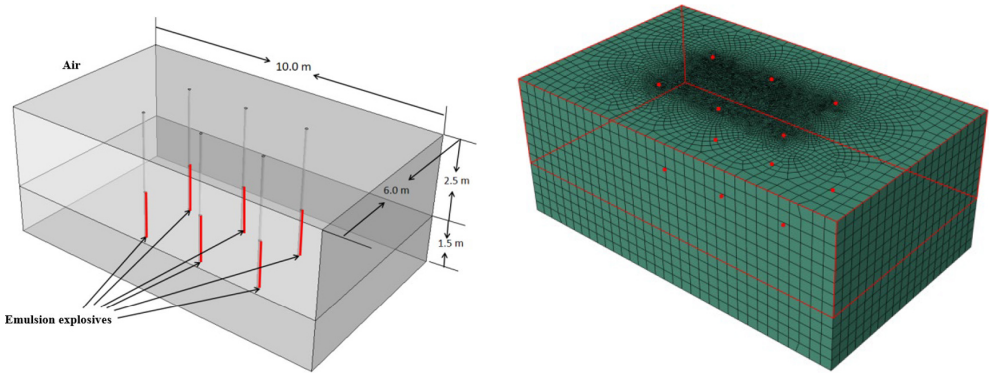

(a) (b)

Fig. 3. Euler body model for six hole blasting: (a) Dimension settings, (b) Meshing

3.2.3. JWL Blasting Model Theory

For explosion simulations, many different equations of state have been proposed to describe the products of explosions, among which the JWL (Jones-Wilkins-Lee) equation of state [19,20] is considered the most comprehensive. The JWL equation of state was introduced in the 1960s by Japanese scientist John Paul Wierzbicki and British scientist John Wilkins. This equation effectively models the change in strain energy of materials under compressive loads. It is used to describe the dynamic behavior of materials under high pressure, high temperature, and high strain rates, making it particularly suitable for material behavior analysis under dynamic loading conditions such as high-speed impacts and explosions. The JWL equation of state is widely used in numerical simulations and has the following form:

$$P = Ae^{-R_1 V} + Be^{-R_2 V} + CV^{-(1+\omega)} \tag{3.3}$$

Where A, B, C, R_1, R_2 and ω are explosion constants, and V is the relative volume v_1/v_2. These constants can be derived by comparing results from hydrodynamic calculations and cylindrical metal expansion tests (cylinder tests). Figure 4 illustrates the impact of each parameter in Eq. (3.3) on the P–V curve.

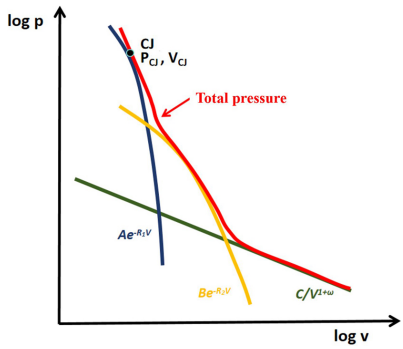

Fig. 4. Influence curve of various parameters on adiabatic pressure in JWL EOS

Since the explosion products are very hot in the initial phase, the gases are in an adiabatic expansion state (passing through the CJ point). Subsequently, as they expand rapidly, the behavior of the explosion products approximates that of an ideal gas. The energy contained in the explosion products under given expansion conditions is as follows:

$$e = \frac{A}{R_1} e^{-R_1 V} + \frac{B}{R_2} e^{-R_2 V} + \frac{C/\omega}{V^{\omega}} \tag{3.4}$$

The above two formulas share the same parameters, and by combining the equations, the JWL equation of state incorporating energy terms can be derived as follows:

$$P = A\left(1 - \frac{\omega}{VR_1}\right) e^{-R_1 V} + B\left(1 - \frac{\omega}{VR_2}\right) e^{-R_2 V} + \frac{\omega e}{V^{\omega}} \tag{3.5}$$

The parameters in this equation, as well as the pressure and energy generated per unit volume of explosion products under the CJ conditions and the detonation velocity, can be input into ABAQUS as input parameters.

3.3. Numerical calculation model parameters

3.3.1. JH-2 constitutive model parameters

The JH-2 material parameters for slightly weathered and moderately weathered granite in the thesis are selected from literature [16], as shown in Table 3.

Table 3. Granite JH-2 Parameters

	Slightly Weathered Granite	**Moderately Weathered Granite**
ρ (kg/m^3)	2540	2520
G (GPa)	12.31	6.62
A	0.82	0.56
B	0.27	0.19
N	0.67	0.59
C	0.005	0.005
M	0.67	0.59
$\dot{\varepsilon}_0$	1	1
T (MPa)	48	31
D_1	0.006	0.007
D_2	0.9	0.8
HEL (GPa)	4.5	4.5
K_1	44.65	22.51
K_2	–267.20	–182.50
K_3	1132.50	830.00
P_{HEL} (GPa)	2.36	2.26

3.3.2. JWL emulsion explosive parameters

In ABAQUS, the JWL model is used to model and analyze the behavior of materials under dynamic loading conditions such as impact and explosion. This can simulate the pressure-volume relationship, energy release rate, and fracture behavior of materials, thereby predicting the response and failure of materials under dynamic loading.

Since determining the JWL parameters requires complex and precise experiments, this study references the JWL parameters for emulsion explosives obtained by Sanchidrian J.A. through cylinder test expansion data [21]. The specific data are shown in Table 4.

Table 4. Parameters of Emulsion Explosives

ρ (kg/m^3)	Detonation Wave Velocity (m/s)	A (MPa)	B (MPa)	ω	R_1	R_2	Explosion Energy Density (J/kg)
1630	6930	557600	5350	0.35	6.01	1.07	6060000

3.3.3. JWL air parameters

In ABAQUS, when it is necessary to define the properties of air or other gases, such as in thermal analysis or fluid dynamics analysis, it is required to define the equation of state of the gas, specific heat, and dynamic viscosity. The equation of state for the gas includes the gas constant R and the ambient pressure P. The gas constant R is an important parameter used in the ideal gas equation $PV = nRT$ [22], where P is pressure, V is volume, n is the number of moles of gas, T is temperature, and R is the gas constant. For air, its gas constant can be obtained by dividing the universal gas constant by the average molar mass of air (Table 5).

Table 5. Air Parameters

ρ (kg/m^3)	Gas Constant	Ambient Pressure (Pa)	Specific Heat	Dynamic Viscosity
1.01	287	10100	717.7	1.81×10^{-5}

3.4. Numerical calculation steps and analysis methods

To comprehensively simulate the damage patterns of two weathering degrees of granite under different in-situ stresses during blasting, a series of detailed numerical simulations were performed using the ABAQUS finite element analysis software. This section will introduce the key steps of the entire numerical analysis process to ensure accurate and reliable simulation results. The main steps of the numerical analysis process are as follows: (1) Analysis Step Settings: Use dynamic explicit analysis, setting up two analysis steps. Step-1: Simulate different confining pressures by importing pre-stress fields to represent various in-situ stress conditions. Step-2: Blasting simulation analysis step. Based on the review of various research test simulation results and accuracy calculations [23], the duration of the analysis step is set to 4 ms. (2) Boundary Conditions: To simulate rock blasting under the influence of in-situ stress, apply corresponding pressures on all faces of the model except the blast hole surface. The static

pressure in the Y direction represents vertical in-situ stress, while the static pressure in the X–Z directions represents horizontal in-situ stress. (3) In-Situ Stress Equilibrium: To maximally restore the natural in-situ stress state, use a static general analysis step. Apply static stress on the boundaries of the rock mass model with the same mesh division, then run the model to obtain the ODB file. In the dynamic explicit analysis step's load module, create a pre-stress field and select the ODB file. Configure the analysis step data, defining the loading steps and time points. Finally, rerun the model to obtain the initial in-situ stress of each rock element before blasting. (4) Contact: Set general contact (Explicit) between parts. Define contact properties with tangential behavior and normal behavior. Use the "Penalty" friction formulation with a friction coefficient of 0.1, and set the contact property to "hard contact". (5) Calling the UMAT Subroutine: In the material module, call the user material (UMAT), setting the number of material properties to 32. Enable the use of dependent solution state variables, setting 8 state variables. Generate an input file, incorporating the JH-2 model parameters and output variables by referencing the JH-2 model text.

4. Analysis of granite blasting damage and cracking patterns

The damage cloud chart generated by the JH-2 model provides an intuitive tool for studying rock mass damage. Through the use of colors and graphics, it clearly expresses the degree of damage in different regions and visually shows the distribution of internal damage within the rock mass. This helps in understanding the damage state of the rock mass after being subjected to force. Therefore, by analyzing the damage characteristics of moderately weathered and slightly weathered granite, research on the patterns of damage and cracking in granite due to blasting can be conducted.

4.1. Blasting damage and cracking patterns in moderately weathered granite

4.1.1. Damage rupture pattern

To investigate the longitudinal damage and cracking patterns of moderately weathered granite, the X–Z cross-section of the model was analyzed. Figure 5 shows the longitudinal damage and fracture cloud chart of moderately weathered granite under blasting. The observations from the chart are as follows: (1) Blasting at 20 m Depth: The rock mass experienced extensive damage and destruction, with almost all the rock between blast holes being damaged, which can be considered as overall cracking. The intrusion depth at the bottom of the blast hole reached the bottom of the rock mass. (2) Blasting at 200 m Depth: The longitudinal damage significantly decreased, and the overall shape of the blasting damage formed a conical pattern. The intrusion depth at the bottom of the blast hole decreased. (3) Blasting at 500 m Depth: The cracks increased and connected the blast holes, longitudinally dividing the rock mass into larger fragments. There was no significant change in the intrusion depth at the bottom of the blast hole. (4) Blasting at 1000 m Depth: The longitudinal damage further intensified, and crack propagation increased. The overall intrusion depth pattern at the bottom of the blast hole was similar to that at 500 meters.

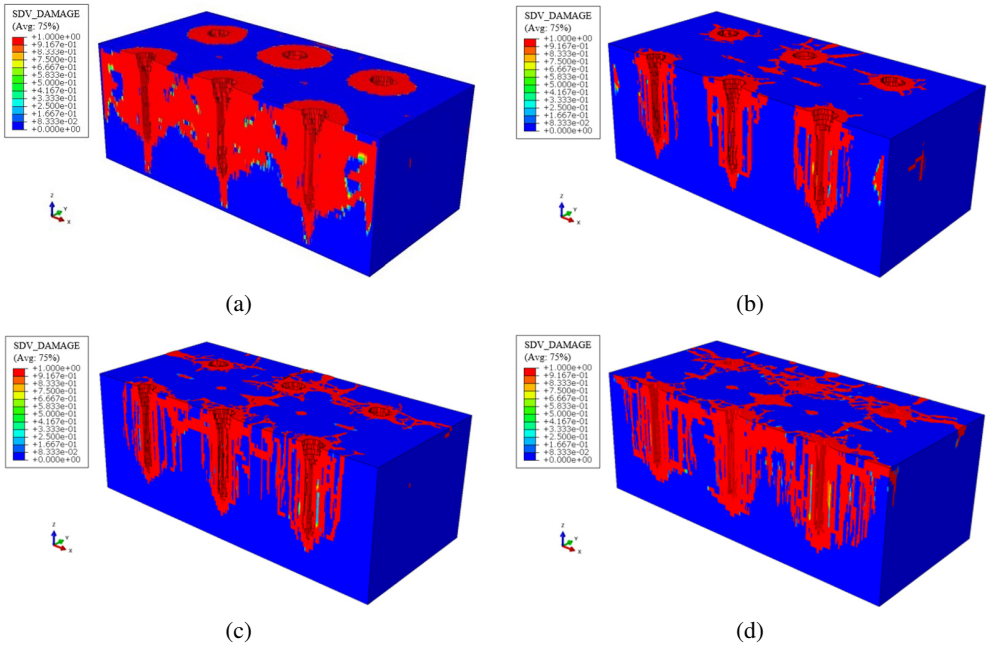

Fig. 5. Longitudinal damage rupture cloud of moderately weathered granite blasting: (a) 20 m, (b) 200 m, (c) 500 m, (d) 1000 m

4.1.2. Law of plastic failure

Due to the damage parameter D value of 1 being unable to effectively distinguish between large deformations and minor cracks in the rock mass, a plastic strain cloud chart for moderately weathered granite was created to more intuitively describe the degree of damage and deformation in different regions using the JH-2 constitutive model, as shown in Figure 6. Since the JH-2 constitutive model simulates brittle materials, according to reference [20], the ultimate elastic strain of granite is 0.5%. When the equivalent plastic strain exceeds this value, it can be considered as fracture damage. In the output cloud chart, the maximum value of the plastic strain cloud chart is set to 10%. By comparing the size of the equivalent plastic strain, the crack propagation mechanism of granite during blasting can be observed. The observations from the chart are as follows: (1) Blasting at 20 m Depth: The damage and fracture trend of moderately weathered granite at a depth of 20 meters shows an outward spread from the blast hole. When the inner circle's plastic strain exceeds 10%, it usually indicates that the moderately weathered granite in that region has been completely fractured. The region with a plastic strain of approximately 5% represents extensive and dense crack propagation, meaning that the plastic strain is relatively high on the inner side of the blast hole and gradually decreases towards the edges. (2) Blasting at 200 m Depth: At a depth of 200 meters, the damage and fracture trend of moderately weathered granite shows an expansion from the central blast hole towards the edges. The cracks between blast holes connect and divide the rock mass into

larger rock fragments. (3) Blasting at Greater Depths (500 m and 1000 m): As the in-situ stress increases with greater depth, such as at 500 meters, the area of the completely fractured region (with plastic strain greater than 10%) decreases, while the number of minor cracks with lower plastic strain significantly increases. At a depth of 1000 meters, the overall plastic strain decreases, and the number of minor cracks increases, indicating that as the depth increases, the fracturing mode of the rock mass tends to become more fragmented.

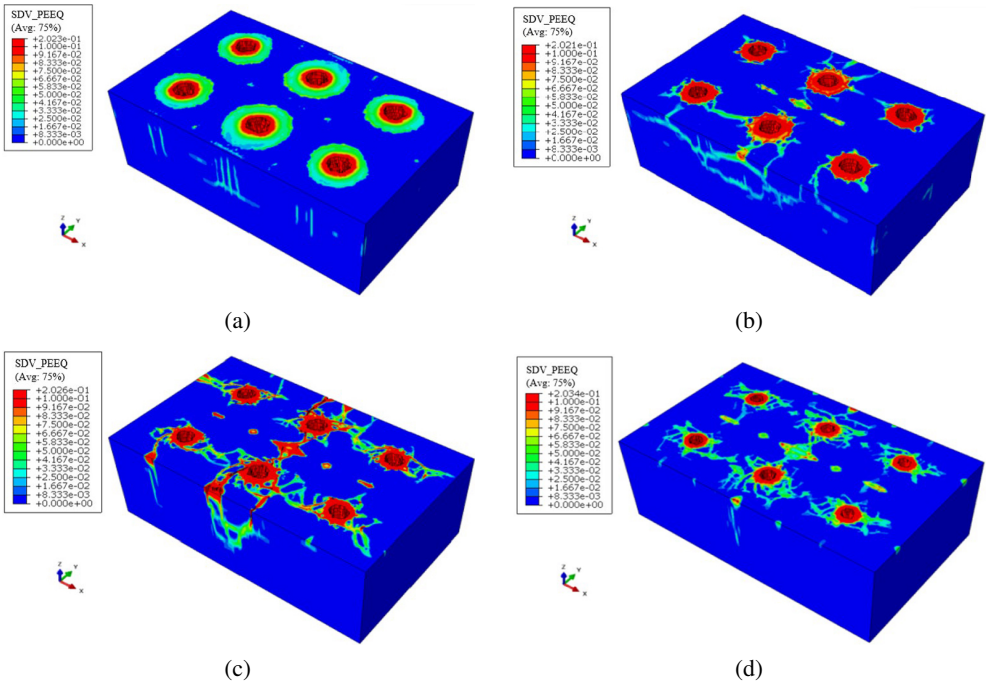

Fig. 6. Plastic strain cloud map of slightly weathered granite under stress at different depths: (a) 20 m, (b) 200 m, (c) 500 m, (d) 1000 m

4.1.3. Percentage of damage rupture

To more intuitively describe the damage and fracture characteristics of moderately weathered granite under blasting at different depths, the ratio of the damaged area to the total model area was calculated and plotted as the damage proportion in moderately weathered granite blasting, as shown in Figure 7. The damage proportion is defined as the ratio of the damaged area (where the D value is 1) to the surface area of the rock mass model. The observations from the chart are as follows: (1) Damage Proportion at Different Depths: At a blasting depth of 20 meters, the damage in moderately weathered granite is greater compared to other depths. As the depth increases from 20 meters to 200 meters, the reduction in damage proportion at each blast hole depth is 35.48%, 43.60%, 53.44%, and 64.92%, respectively, which is significantly larger than the changes under other in-situ stress conditions. (2) Maximum and Minimum Damage: The

maximum damage on the blast hole surface and bottom (at depths of 0 meters and 1.5 meters) occurs at a blasting depth of 20 meters, with values of 30.99% and 35.63%, respectively. The minimum damage occurs at a blasting depth of 200 meters, with values of 20.02% and 12.49%, respectively. As the depth increases from 20 meters to 200 meters, the damage on the blast hole surface and bottom decreases. However, as the depth increases from 200 meters to 1000 meters, the damage on the blast hole surface and bottom increases. (3) Internal Damage at Different Depths: The maximum damage in the internal regions of the blast hole (at depths of 0.5 meters and 1.0 meters) occurs at a blasting depth of 200 meters, with values of 53.93% and 61.22%, respectively. The minimum damage occurs at a blasting depth of 500 meters, with values of 25.22% and 9.49%, respectively. As the depth increases from 20 meters to 500 meters, the damage on the blast hole surface and bottom decreases. However, as the depth increases from 500 meters to 1000 meters, the damage on the blast hole surface and bottom increases.

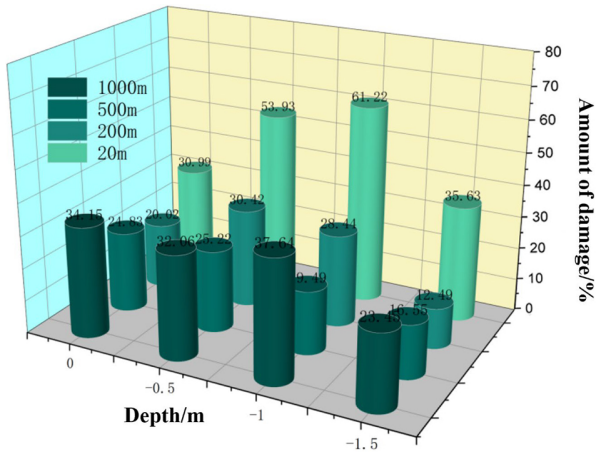

Fig. 7. Column chart of the proportion of damage to moderately weathered granite

4.2. Blasting damage and cracking patterns in slightly weathered granite

4.2.1. Damage rupture pattern

To investigate the longitudinal damage and cracking patterns of slightly weathered granite, the X–Z cross-section of the model was analyzed. Figure 8 shows the longitudinal damage and fracture cloud chart of slightly weathered granite under blasting. The observations from the chart are as follows: (1) Blasting at 20 m Depth: The longitudinal damage in the rock mass exhibits a "T" shape, with significant damage on the blasting surface and less damage within the rock mass. (2) Blasting at 200 m Depth: The damage distribution is more uniform, with a noticeable reduction in damage on the blasting surface. There is more longitudinal crack propagation, dividing the rock mass around the blast hole into long strips along the X direction. (3) Blasting at 500 m Depth: There is no significant change except for a slight reduction in the number of cracks. (4) Blasting at 1000 m Depth: Longitudinal damage significantly decreases,

with almost no longitudinal crack propagation within the rock mass. The intrusion depth at the bottom of the hole also significantly reduces, indicating a marked decrease in blasting effectiveness under the in-situ stress conditions at this depth.

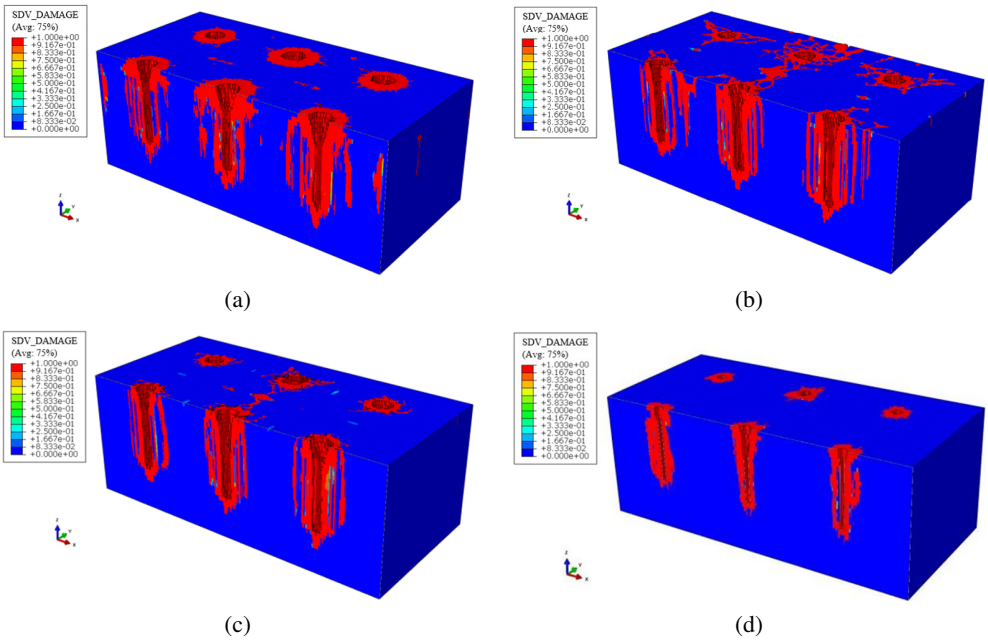

Fig. 8. Longitudinal damage cloud map of slightly weathered granite: (a) 20 m, (b) 200 m, (c) 500 m, (d) 1000 m

4.2.2. Law of plastic failure

Similarly, the plastic strain cloud chart for slightly weathered granite was plotted, as shown in Figure 9. The observations from the chart are as follows: (1) Blasting at 20 m Depth: Similar to moderately weathered granite, the damage trend in slightly weathered granite at a depth of 20 meters shows an outward spread from the blast hole, resulting in complex and dense crack propagation. Outside the plastic damage zone, a circular arc with a plastic strain greater than 10% is formed, distributed along the inner side of the rock mass. This is due to stress waves from adjacent blast holes being transmitted to this region, causing secondary damage to the rock mass. (2) Blasting at 200 m Depth: At this depth, the number of small strain cracks with plastic strain less than 5% increases. Crack propagation mainly occurs from the blast hole in the Y direction, longitudinally splitting the rock mass. (3) Blasting at 500 m Depth: The area of completely fractured zones around the blast hole does not show significant changes, but the number of small strain cracks decreases. (4) Blasting at 1000 m Depth: The plastic strain around the blast hole significantly decreases, and small strain cracks are only distributed around the blast hole.

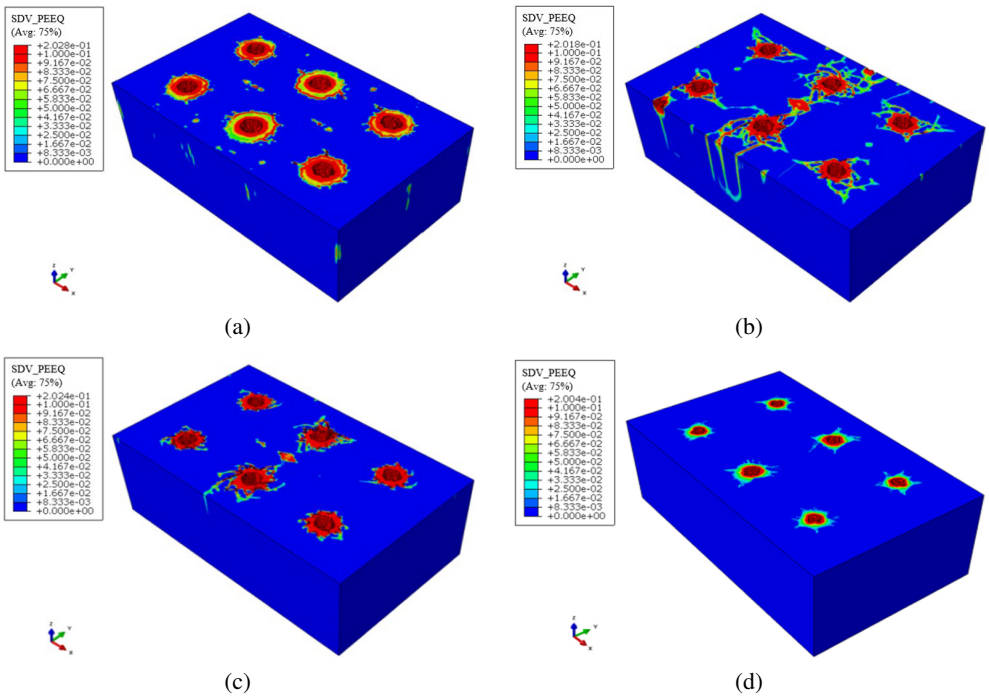

Fig. 9. Plastic strain cloud map of slightly weathered granite under stress at different depths: (a) 20 m, (b) 200 m, (c) 500 m, (d) 1000 m

4.2.3. Percentage of damage rupture

To more intuitively describe the damage and fracture characteristics of moderately weathered granite under different depth conditions, the ratio of the damaged area to the total model area was calculated and plotted as the damage proportion in moderately weathered granite blasting, as shown in Figure 10. The observations from the chart are as follows: (1) Damage at Blast Hole Interior (0.5 m and 1.0 m): Unlike moderately weathered granite, under 20 m depth in-situ stress conditions, the damage in slightly weathered granite is significantly greater within the blast hole (at depths of 0.5 m and 1.0 m) compared to other blasting depths. The damage proportions are 34.87% and 35.31%, respectively. The smallest damage occurs at a blasting depth of 1000 meters, with values of 12.57% and 12.03%, respectively. As the depth increases from 20 m to 1000 m, the damage within the blast hole uniformly decreases. (2) Damage at Blast Hole Surface and Bottom (0 m and 1.5 m): The maximum damage at the blast hole surface and bottom occurs at a depth of 200 meters, with values of 30.99% and 35.63%, respectively. The minimum damage also occurs at a depth of 1000 meters, with values of 12.40% and 10.18%, respectively. This trend is opposite to that observed in moderately weathered granite. As the depth increases from 20 m to 200 m, the damage at the blast hole surface and bottom increases. However, as the depth further increases to 1000 m, the damage decreases.

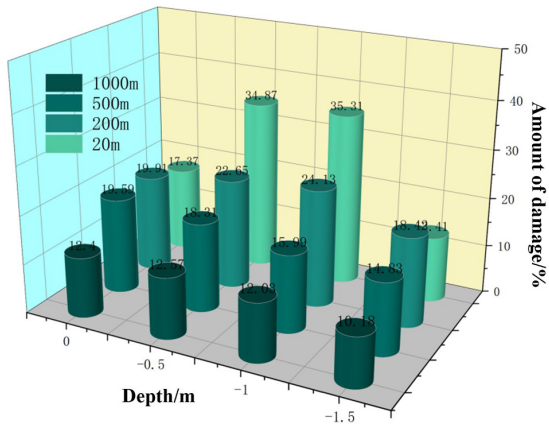

Fig. 10. Proportion of Blast Hole Damage in Slightly Weathered Granite at Different Depths

5. Conclusions

This study, based on the blasting engineering of the Danshan subway station on Qingdao Metro Line 15, investigates the cracking and damage patterns during the blasting construction of moderately weathered and slightly weathered granite. Using the ABAQUS large-scale finite element program, a series of rectangular six-hole models were established. The CEL (Coupled Eulerian–Lagrangian) method was employed to simulate the propagation of shock waves in space after explosive detonation. The in-situ stress states of granite at different depth gradients were analyzed to study the extent and degree of granite damage caused by blasting. The main conclusions are as follows: (1) Using the CEL (Coupled Eulerian–Lagrangian) method, the Eulerian part is divided into Eulerian and Lagrangian elements. The Eulerian domain is set as air material, and the Lagrangian domain is set as TNT to simulate the propagation of shock waves in space after explosive detonation. This approach was employed to analyze the in-situ stress states of granite under different depth gradient conditions and to study the extent and degree of granite damage caused by blasting. The feasibility of this method and the research conclusions provide valuable guidance for engineering blasting practices. (2) When blasting at different depths, the longitudinal damage patterns of moderately weathered and slightly weathered granite exhibit both significant differences and similarities. At shallower depths, the damage modes differ: moderately weathered granite shows overall cracking, while slightly weathered granite displays a “T” shape damage pattern. As the blasting depth increases, the longitudinal damage in slightly weathered granite gradually decreases, whereas the trend in moderately weathered granite is the opposite. This indicates that granites with different degrees of weathering respond complexly to blasting depth and in-situ stress. (3) Opposite Damage Trends at 200 m to 500 m Depths: When the blasting depth increases from 200 meters to 500 meters, the trend in damage quantity for slightly weathered granite is opposite to that of moderately weathered granite. As the blasting depth increases, the difference in damage quantities at various depths of the blast hole gradually decreases.

References

[1] CURTA (China Urban Railway Transportation Association), "Action Program for Green Urban Railway Development in China's Urban Railway Transportation", *China Metros*, vol. 08, pp. 20–35, 2022.

[2] F. Zhang, J. Peng, G. Fan, S. Li, and Y. Li, "Mechanisms of blasting-induced rock fractures under different static stress and joint properties conditions", *Rock and Soil Mechanics*, vol. 07, pp. 1839–1846, 2016.

[3] S. Liu, Z. Wang, Y. Zhang, M. Kou and J. Bi, "The phase-field simulations of blasting failure in granites", *International Journal of Impact Engineering*, vol. 167, art. no. 104274, 2022, doi: 10.1016/j.ijimpeng.2022.104274.

[4] H. Wang, et al., "Effect of confining pressure on damage accumulation of rock under repeated blast loading", *International Journal of Impact Engineering*, vol. 15, art. no. 103961, 2021, doi: 10.1016/j.ijimpeng.2021.103961.

[5] Z. Wang, H. Wang, J. Wang, and N. Tian, "Finite element analyses of constitutive models performance in the simulation of blast-induced rock cracks", *Computers and Geotechnics*, vol. 135, art. no. 104172, 2021, doi: 10.1016/j.compgeo.2021.104172.

[6] J. Wang, Y. Yin, and C. Luo, "Johnson–Holmquist-II(JH-2) Constitutive Model for Rock Materials: Parameter Determination and Application in Tunnel Smooth Blasting", *Applied Sciences*, vol. 8, no. 9, art. no. 1675, 2018, doi: 10.3390/app8091675.

[7] P. Baranowski, et al., "Fracture and fragmentation of dolomite rock using the JH-2 constitutive model: Parameter determination, experiments and simulations", *International Journal of Impact Engineering*, vol. 140, art. no. 103543, 2020, doi: 10.1016/j.ijimpeng.2020.103543.

[8] T. Li, A. Fei, X. Niu, and C. Zhu, "Numerical simulation of blasting at different positions of granite by different explosives", *Engineering Blasting*, vol. 4, pp. 8–15, 2019.

[9] H. An, Y. Song, and D. Yang, "Experimental study of the effect of rock blasting with various cutting forms for tunnel excavation using physical model tests", *Archives of Civil Engineering*, vol. 67, no. 3, pp. 599–618, 2021, doi: 10.24425/ace.2021.138073.

[10] F. Jing, Q. Sheng, Y. Zhang, and Y. Liu, "Statistical analysis of geostress distribution laws for different rocks", *Rock and Soil Mechanics*, vol. 7, pp. 1877–1883, 2008.

[11] G. Johnson and W. Cook, "A constitutive model and data for metals subjected to large strains, high strain rates and high temperatures", in *Proceedings of the Seventh International Symposium on Ballistics, Hague, The Netherlands*. ADPA, 1983, pp. 541–547.

[12] G. Johnson and T. Holmquist, "A computational constitutive model for brittle materials subjected to large strains, high strain rates and high pressures", in *Shock Wave and High-Strain-Rate Phenomena in Materials*, 1st ed., M.A. Meyers and L.E. Murr, Eds. Boca Raton, FL, USA: CRC Press, 1992, pp. 1075–1081.

[13] G. Johnson and T. Holmquist, "An improved computational constitutive model for brittle materials", *AIP Conference Proceedings*, vol. 309, no. 1, pp. 981–984, 1994, doi: 10.1063/1.46199.

[14] T. Holmquist, G. Johnson, C. Lopatin, D. Grady, and E. Hertel, "High strain rate properties and constitutive modeling of glass", in *Proceedings of the 15th International Symposium on Ballistics*. 1995, pp. 21–24.

[15] G. Johnson and T. Holmquist, "Response of boron carbide subjected to large strains, high strain rates, and high pressures", *Journal of Applied Physics*, vol. 85, no. 12, pp. 8060–8073, 1999, doi: 10.1063/1.370643.

[16] T. Holmquist, G. Johnson, and W. Cook, "A constitutive model and data for concrete subjected to large strains, high strain rates and high pressures", in*Proceedings of the 14th International Symposium on Ballistics*. 1993, pp. 26–29.

[17] F. Li, K. Wu, S. Li, C. Wang, Y. Liu, and Z. Dou, "Study on the dynamic response characteristics of lining structures in large-section tunnel blasting using JH-2 model analysis", *Scientific Reports*, vol. 14, art. no. 10506, 2024, doi: 10.1038/s41598-024-60918-6.

[18] W. Noh, "CEL: A time-dependent, two-space-dimensional, coupled Eulerian–Lagrange code", Technical Report, Livermore, CA (United States): Lawrence Livermore National Lab, 1963.

[19] J. Yang, G. Ren, Q. Yu, and Z. Chen, "Wedge Theory of Rock Fragmentation for Bench Blasting and its Numerical Simulation", in *Proceedings 11th International Symposium on Rock Fragmentation by Blasting*. Melbourne: The Australasian Institute of Mining and Metallurgy, 2015, pp. 169–176.

[20] J. Kury, H. Hornig, E. Lee, et al., "Metal acceleration by chemical explosives", *The Fourth Symposium (International) on Detonation*. 1965, pp. 3–13.

[21] E. Lee, M. Finger, W. Collins, "JWL equation of state coefficients for high explosives", Technical Report, Livermore, CA (United States): Lawrence Livermore National Lab, 1973.

[22] J. Sanchidrian, R. Castedo, L. Lopez, P. Segarra, and A.P. Santos, "Determination of the JWL constants for ANFO and emulsion explosives from cylinder test data", *Central European Journal of Energetic Materials*, vol. 12, no. 2, pp. 177–194, 2015.

[23] C. Borgnakke and R. Sonntag, *Fundamentals of thermodynamics*. John Wiley & Sons, 2020.

[24] X. Li, K. Liu, J. Yang, and R. Song, "Numerical study on blast-induced fragmentation in deep rock mass", *International Journal of Impact Engineering*, vol. 170, art. no. 104367, 2022, doi: 10.1016/j.ijimpeng.2022.104367.

Received: 2024-07-14, Revised: 2024-09-24